

Supporting Information

Intra-cluster energy transfer editing in a dual-emitting system to tap into lifetime thermometry

Claudia M. S. Calado[†], Diogo A. Gálico[†], Muralee Murugesu^{†}*

[†]Department of Chemistry and Biomolecular Sciences, University of Ottawa, Ottawa, Ontario K1N 6N5, Canada.

*Corresponding Author: M. Murugesu (E-mail: m.murugesu@uottawa.ca)

Materials and synthesis

All chemicals were purchased and of reagent grade. All manipulations were performed under aerobic conditions. In a typical synthesis of $\{\text{Ln}_{20}\}$ molecular cluster-aggregate (MCA), 1.00 mmol of $\text{Ln}(\text{NO}_3)_3 \cdot 6\text{H}_2\text{O}$ ($\text{Ln} = \text{Eu}$ or Tb , according to the doping mol % displayed in Table 1) and 1.00 mmol of 6-chloro-2-pyridinol (130 mg) were added to 20 mL of MeOH/MeCN (1:1). After solubilization, 1.00 mmol of triethylamine (139 μL) was added to the solution. The system was kept closed under stirring for 12 hours. At the end of this time, the vial was left open and undisturbed for solvent slow evaporation, and pale-yellow crystals were obtained in the following 5 days with yields around 25% (based on Tb^{III}).

Table S1. Composition of synthesized MCAs, alongside with nominal percentages and experimental values obtained using ICP-OES. $\text{Ln}^{\text{III}} = \text{Gd}^{\text{III}}$ or Eu^{III} .

Composition	$\text{Ln}(\text{NO}_3)_3 \cdot 6\text{H}_2\text{O}$	$\text{Tb}(\text{NO}_3)_3 \cdot 6\text{H}_2\text{O}$	Nominal / %		Experimental / %	
	/ mg	/ mg	Ln^{III}	Tb^{III}	Ln^{III}	Tb^{III}
$\{\text{Eu}_1\text{Tb}_{19}\}$ (1)	22	430	5	95	4.93	95.07
$\{\text{Eu}_2\text{Tb}_{18}\}$ (2)	45	408	10	90	9.93	90.07
$\{\text{Eu}_3\text{Tb}_{17}\}$ (3)	67	385	15	85	14.88	85.12
$\{\text{Eu}_4\text{Tb}_{16}\}$ (4)	89	362	20	80	19.98	80.02
$\{\text{Gd}_1\text{Tb}_{19}\}$ (5)	23	430	5	95	5.12	94.88
$\{\text{Gd}_2\text{Tb}_{18}\}$ (6)	45	408	10	90	10.11	89.89
$\{\text{Gd}_3\text{Tb}_{17}\}$ (7)	68	385	15	85	15.15	84.86
$\{\text{Gd}_4\text{Tb}_{16}\}$ (8)	90	362	20	80	19.83	80.17

Characterizations

Powder X-ray diffraction (PXRD) data were collected in a Bruker D8 Endeavor diffractometer with $\text{CuK}\alpha$ (1.5418 Å) radiation source equipped with LynxEye XE-T silicon strip detector, ranging from 4° to 20° (2θ) and scan speed about 1.1° min^{-1} . Attenuated total reflectance Fourier transform infrared (ATR FT-IR) spectra were obtained in an Agilent Cary 630 spectrometer, ranging from 4000 to 600 cm^{-1} . Energy-dispersive X-ray spectra (EDS) were collected in a JEOL JSM-7500F microscope, samples were supported in double-sided adhesive carbon tape and coated with an 8-nm Au/Pd layer. Inductively coupled plasma optical emission spectrometry (ICP-OES) analysis was performed with an Agilent 5110 ICP-OES instrument.

Photoluminescence studies were carried out in acetonitrile suspension (0.1 mg mL^{-1}). The raw data was obtained in a Horiba QuantaMaster 8075-21 spectrofluorometer equipped with a Hamamatsu R13456 red extended PMT detector. Ozone-free PowerArc energy 75 W continuous xenon lamp was used as radiation source for steady-state measurements. Excitation and emission spectra were corrected according to the optical system. Emission decay curves were obtained with a 150 W flash xenon lamp as radiation source. For all measurements, a cuvette was placed inside a single cuvette Peltier K-155-C. At each temperature change, the system was allowed 15 minutes for stabilization before measurements.

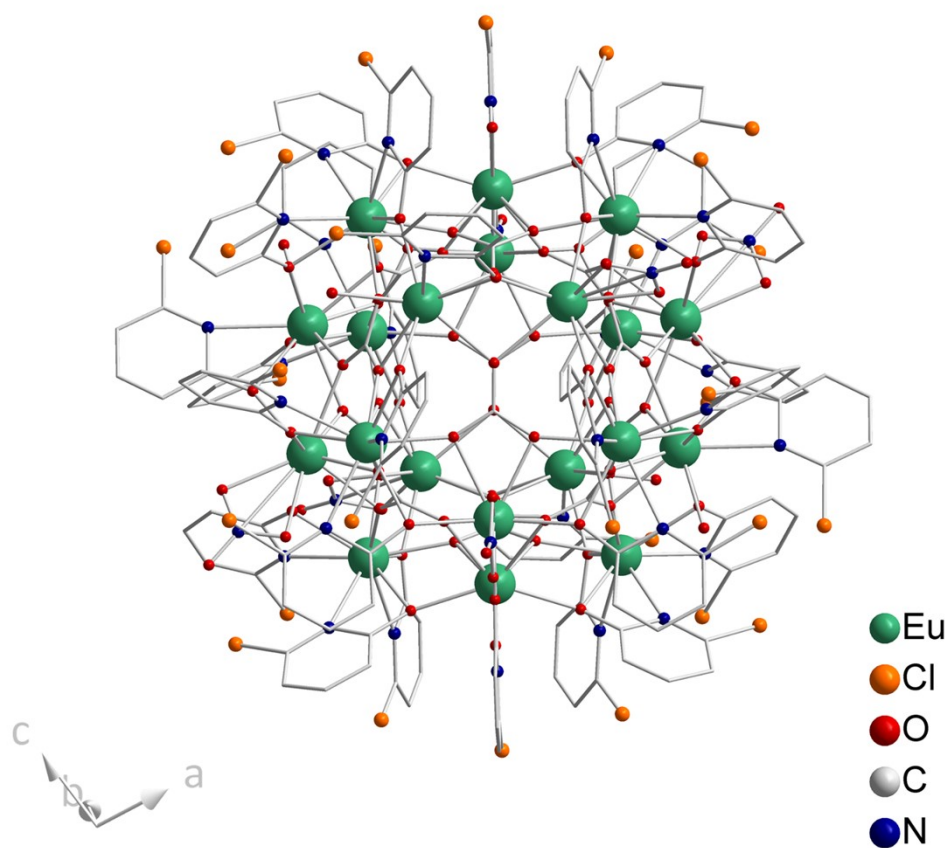


Figure S1. Crystal structure of $\{\text{Eu}_{20}\}$ molecular cluster-aggregate (CCDC 2023766). Hydrogens are omitted for clarity.

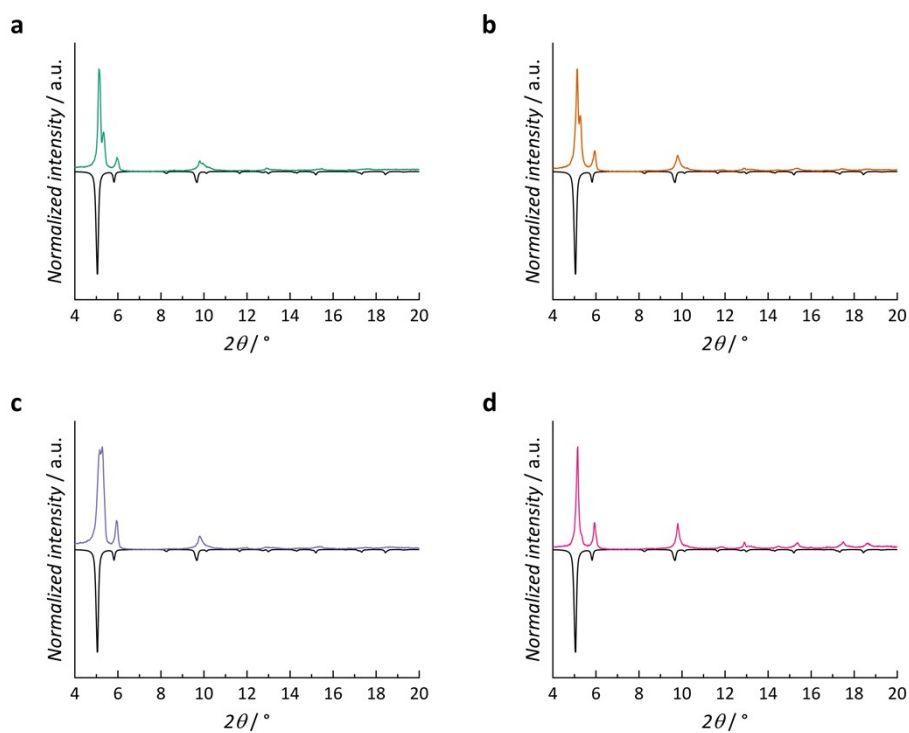


Figure S2. Simulated (black) and experimental diffractograms of **a** $\{\text{Eu}_1\text{Tb}_{19}\}$, **b** $\{\text{Eu}_2\text{Tb}_{18}\}$, **c** $\{\text{Eu}_3\text{Tb}_{17}\}$ and **d** $\{\text{Eu}_4\text{Tb}_{16}\}$. Simulated pattern refers to $\{\text{Eu}_{20}\}$ MCA (CCDC 2023766).

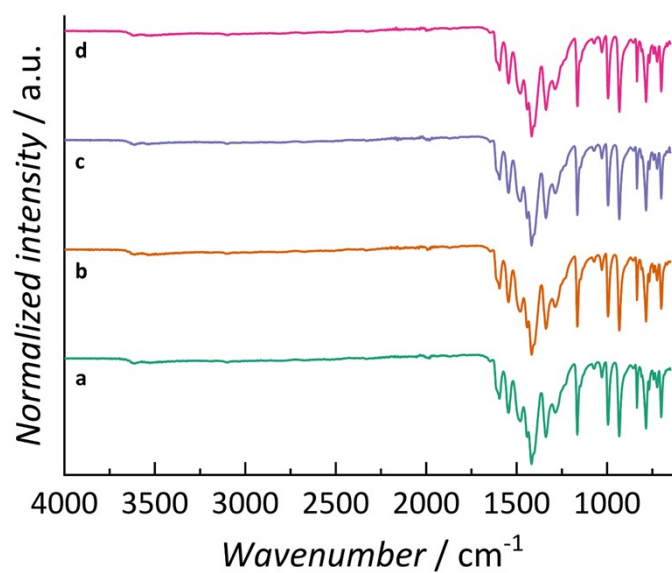


Figure S3. Fourier transform infrared spectra of **a** $\{\text{Eu}_1\text{Tb}_{19}\}$, **b** $\{\text{Eu}_2\text{Tb}_{18}\}$, **c** $\{\text{Eu}_3\text{Tb}_{17}\}$ and **d** $\{\text{Eu}_4\text{Tb}_{16}\}$.

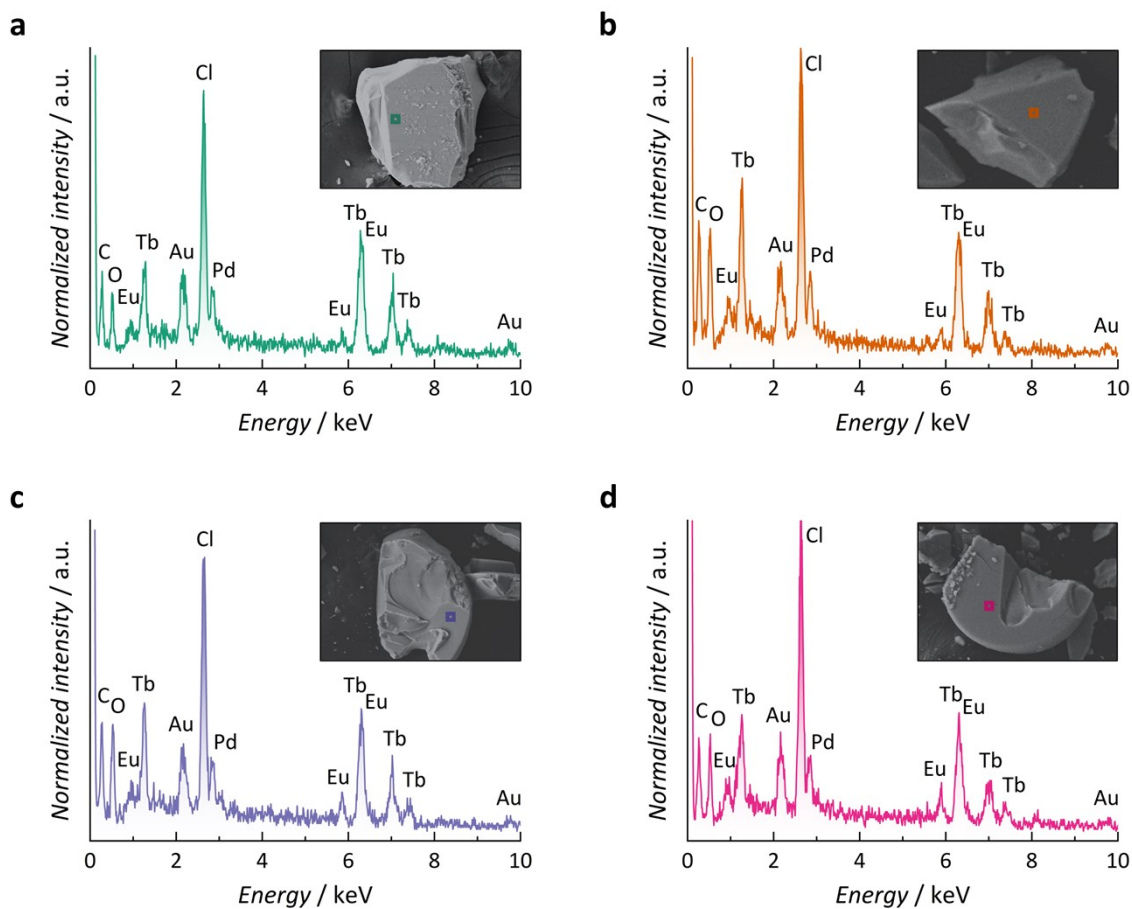


Figure S4. Energy-dispersive X-ray spectra of **a** $\{\text{Eu}_1\text{Tb}_{19}\}$, **b** $\{\text{Eu}_2\text{Tb}_{18}\}$, **c** $\{\text{Eu}_3\text{Tb}_{17}\}$ and **d** $\{\text{Eu}_4\text{Tb}_{16}\}$. SEM images of crystals and respective areas used for EDS measurements are shown in the inserts. Quantification is not possible due to the proximity and overlap of Tb^{III} and Eu^{III} peaks, however there is a visible correlation between relative intensity and composition content.

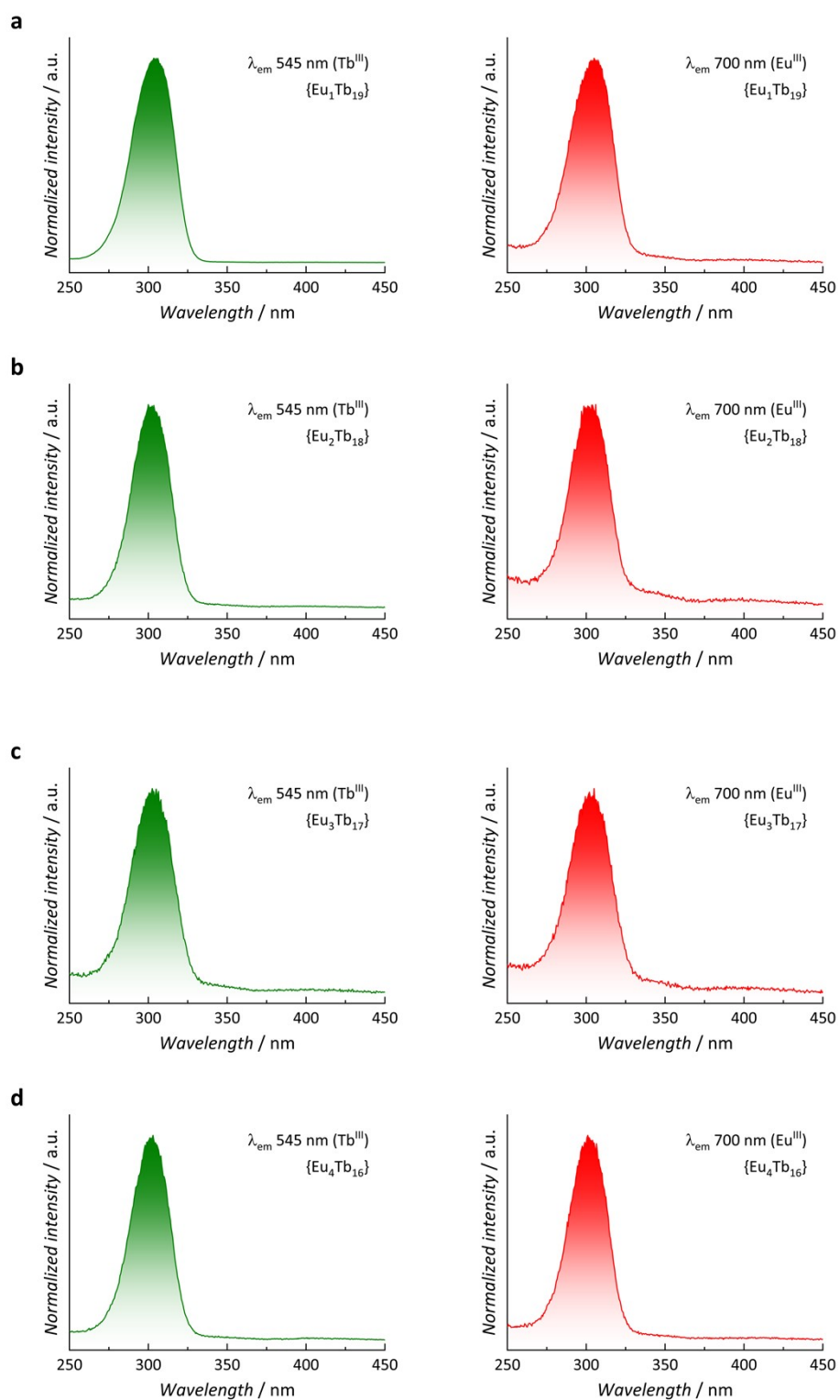


Figure S5. Excitation spectra of **a** {Eu₁Tb₁₉}, **b** {Eu₂Tb₁₈}, **c** {Eu₃Tb₁₇} and **d** {Eu₄Tb₁₆}, collected at 20 °C, monitoring Tb^{III} ⁵D₄→⁷F₅ (545 nm) and Eu^{III} ⁵D₀→⁷F₄ (700 nm) emission bands.

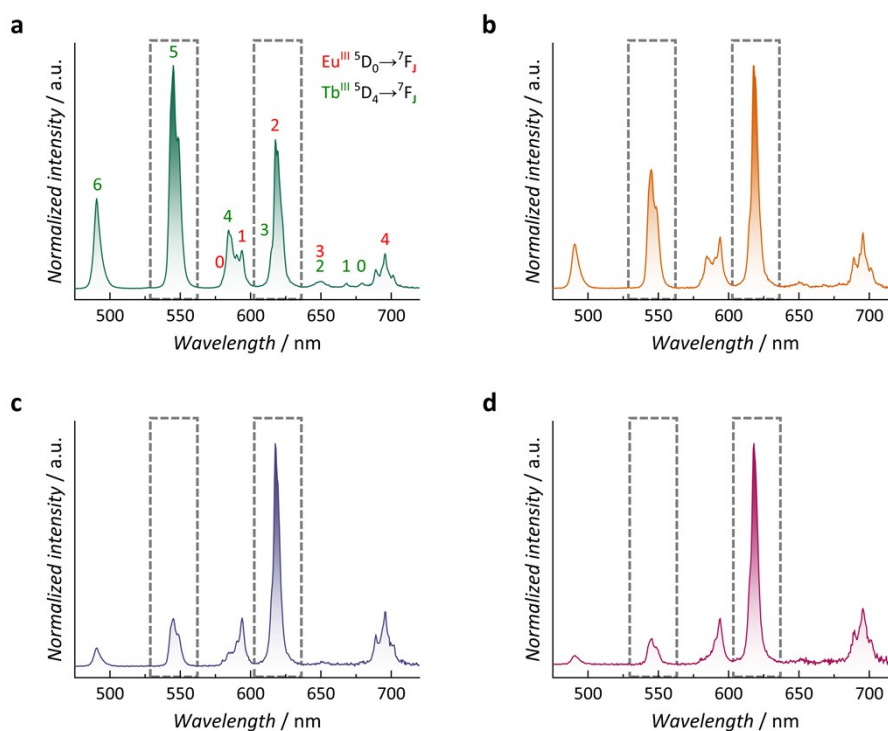


Figure S6. Emission spectra of **a** $\{\text{Eu}_1\text{Tb}_{19}\}$, **b** $\{\text{Eu}_2\text{Tb}_{18}\}$, **c** $\{\text{Eu}_3\text{Tb}_{17}\}$ and **d** $\{\text{Eu}_4\text{Tb}_{16}\}$. Collected at 20 °C, upon 300 nm excitation. Dashed rectangles highlight the intensity ratio of $\text{Tb}^{\text{III}} ({}^5\text{D}_4 \rightarrow {}^7\text{F}_5)$ and $\text{Eu}^{\text{III}} ({}^5\text{D}_0 \rightarrow {}^7\text{F}_2)$ most intense emission bands.

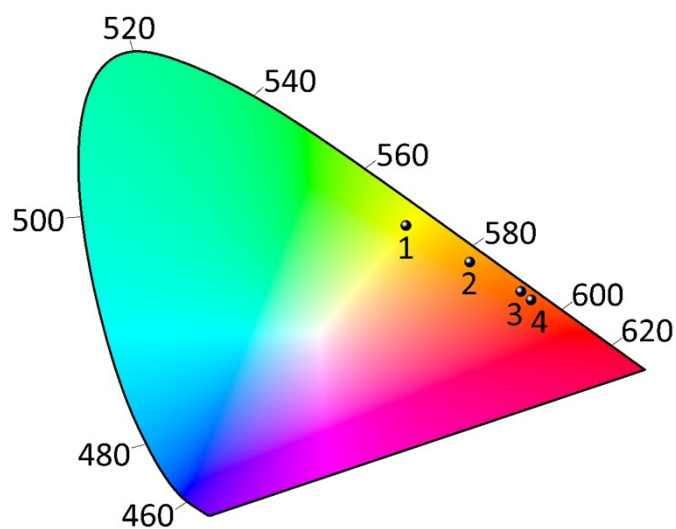


Figure S7. CIE 1931 chromaticity diagram of **1** $\{\text{Eu}_1\text{Tb}_{19}\}$, **2** $\{\text{Eu}_2\text{Tb}_{18}\}$, **3** $\{\text{Eu}_3\text{Tb}_{17}\}$ and **4** $\{\text{Eu}_4\text{Tb}_{16}\}$. Collected at 20 °C, upon 300 nm excitation.

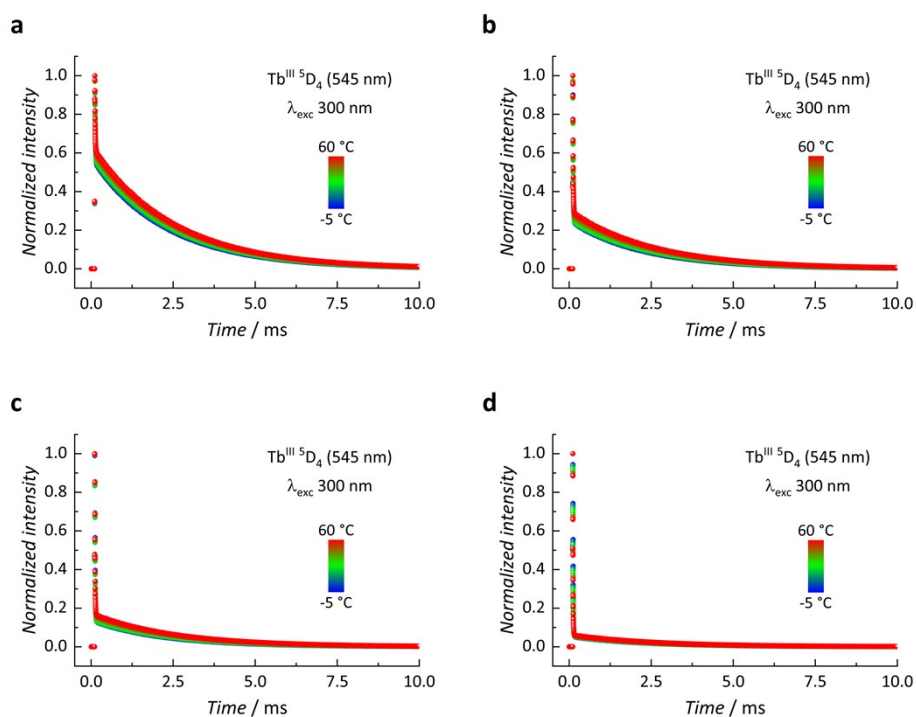


Figure S8. Variable-temperature emission decay curves monitoring $Tb^{III} \ ^5D_4$ (545 nm) of **a** $\{Eu_1Tb_{19}\}$, **b** $\{Eu_2Tb_{18}\}$, **c** $\{Eu_3Tb_{17}\}$ and **d** $\{Eu_4Tb_{16}\}$. Upon 300 nm excitation.

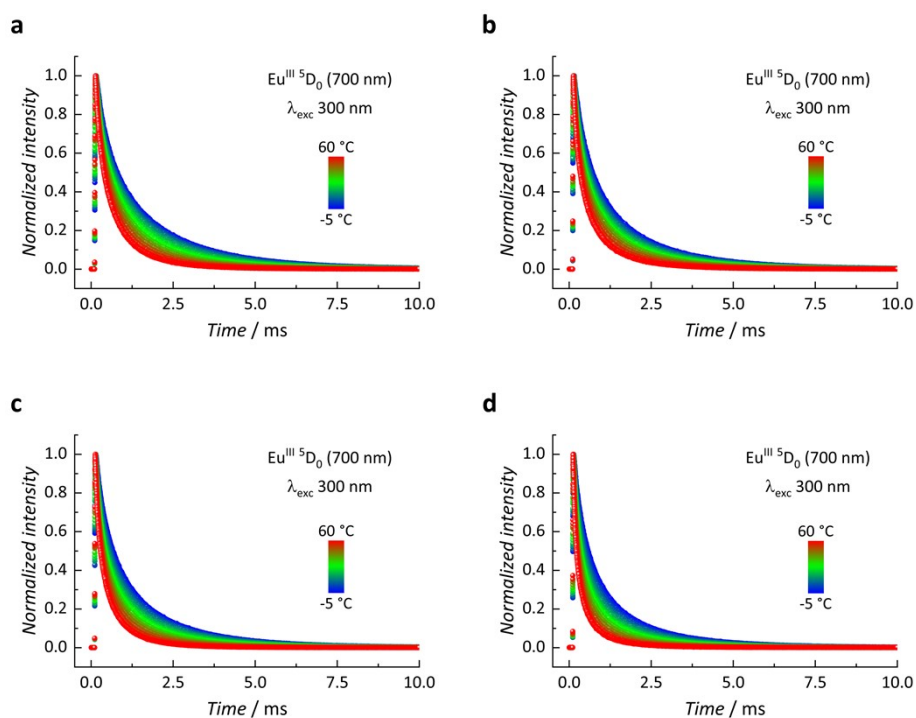


Figure S9. Variable-temperature emission decay curves monitoring $Eu^{III} \ ^5D_0$ (700 nm) of **a** $\{Eu_1Tb_{19}\}$, **b** $\{Eu_2Tb_{18}\}$, **c** $\{Eu_3Tb_{17}\}$ and **d** $\{Eu_4Tb_{16}\}$. Upon 300 nm excitation.

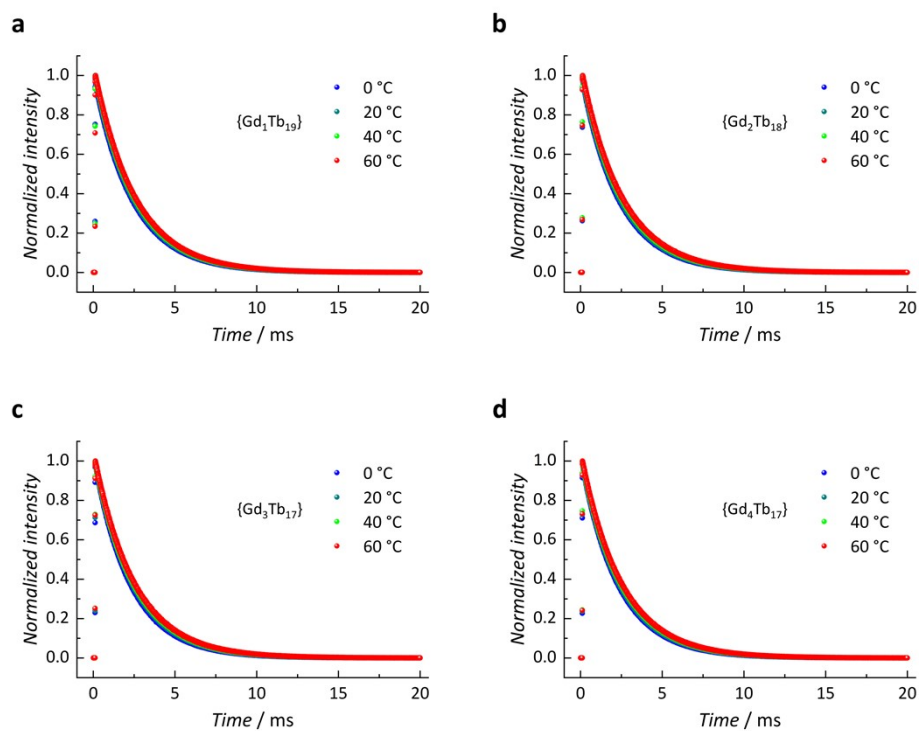


Figure S10. Variable-temperature emission decay curves monitoring $Tb^{III} \ ^5D_4$ (545 nm) of **a** $\{Gd_1Tb_{19}\}$, **b** $\{Gd_2Tb_{18}\}$, **c** $\{Gd_3Tb_{17}\}$ and **d** $\{Gd_4Tb_{16}\}$. Upon 300 nm excitation.

Table S2. Average lifetime (τ) values of Tb^{III} ⁵D₄ (545 nm) and Eu^{III} ⁵D₀ (700 nm) for all MCAs, upon 300 nm excitation, and energy transfer efficiency (η) percentage.

Temperature	MCA	$\tau_{\text{Tb}} / \mu\text{s}$	$\tau_{\text{Eu}} / \mu\text{s}$	Tb ^{III} →Eu ^{III} $\eta_{\text{ET}} / \%$
0 °C	{Eu ₁ Tb ₁₉ }	1227	1267	44.2
	{Eu ₂ Tb ₁₈ }	559	1102	75.2
	{Eu ₃ Tb ₁₇ }	309	1034	86.0
	{Eu ₄ Tb ₁₆ }	134	880	94.0
	{Gd ₁ Tb ₁₉ }	2289	-	-
	{Gd ₂ Tb ₁₈ }	2254	-	-
	{Gd ₃ Tb ₁₇ }	2215	-	-
	{Gd ₄ Tb ₁₆ }	2227	-	-
20 °C	{Eu ₁ Tb ₁₉ }	1342	1049	43.6
	{Eu ₂ Tb ₁₈ }	597	923	74.4
	{Eu ₃ Tb ₁₇ }	332	818	85.7
	{Eu ₄ Tb ₁₆ }	141	660	93.9
	{Gd ₁ Tb ₁₉ }	2382	-	-
	{Gd ₂ Tb ₁₈ }	2331	-	-
	{Gd ₃ Tb ₁₇ }	2314	-	-
	{Gd ₄ Tb ₁₆ }	2315	-	-
40 °C	{Eu ₁ Tb ₁₉ }	1433	800	41.7
	{Eu ₂ Tb ₁₈ }	671	748	72.5
	{Eu ₃ Tb ₁₇ }	383	603	84.1
	{Eu ₄ Tb ₁₆ }	153	467	93.7
	{Gd ₁ Tb ₁₉ }	2459	-	-
	{Gd ₂ Tb ₁₈ }	2443	-	-
	{Gd ₃ Tb ₁₇ }	2404	-	-
	{Gd ₄ Tb ₁₆ }	2413	-	-
60 °C	{Eu ₁ Tb ₁₉ }	1522	563	39.4
	{Eu ₂ Tb ₁₈ }	743	515	70.3
	{Eu ₃ Tb ₁₇ }	425	401	82.8
	{Eu ₄ Tb ₁₆ }	164	309	93.4
	{Gd ₁ Tb ₁₉ }	2514	-	-
	{Gd ₂ Tb ₁₈ }	2498	-	-
	{Gd ₃ Tb ₁₇ }	2470	-	-
	{Gd ₄ Tb ₁₆ }	2471	-	-

Thermometry data treatment

From the temperature-dependent luminescence data, we selected the ratio between τ_{Tb}/τ_{Eu} (ratiometric approach) and τ_{Eu} itself (single approach) as thermometric parameters (Δ). In both cases, the plot of Δ versus temperature can be fitted with a logistic mathematical function (Eq. S1). This equation was used only for fitting purposes and its parameters have no physical meaning. Best-fitting parameters are given in Table S3.

$$y = \frac{A_2 + (A_1 - A_2)}{1 + (x/x_0)^p} \quad (\text{Eq. S1})$$

Relative thermal sensitivity (S_R) curves were obtained by applying the fitted function to Eq. 1, as described in the main manuscript.

To estimate the temperature uncertainty (δT), we first determined the intrinsic percentual error of the instrument when measuring the emission decay curves. In order to do so, we measured the emission decay curves of $Tb^{III} \ ^5D_4$ and $Eu^{III} \ ^5D_0$ in triplicates, at a constant temperature of 20 °C, and calculated their respective lifetime values. A percentual error of less than 1 % was found between runs. This error arises from the instrument electronics and is independent of the temperature. The temperature uncertainty can be obtained from the following equation (Eq. S2),¹ where S_R is the thermal relative sensitivity and $(\delta\tau/\tau) \cdot 100$ is the percentual instrument error (relative uncertainty in the determination of the lifetime):

$$\delta T(T) = \frac{1}{S_R} \cdot \left(\frac{\delta\tau}{\tau} \cdot 100 \right) \quad (\text{Eq. S2})$$

We decided to extrapolate and estimate δT with errors of 1% and 2% (Figure S11). Considering 1 % of error, values around 0.4 – 0.6 °C were estimated for the single approach, while values around 0.4 – 0.5 °C were found for the ratiometric approach. As expected, these values increase with the increase of instrumental error to 2%, being around 0.9 – 1.2 °C for the single approach and 0.7 – 0.9 °C for the ratiometric approach. However, it is valid to point out that δT is greatly influenced by the measurement conditions and instrument setup.

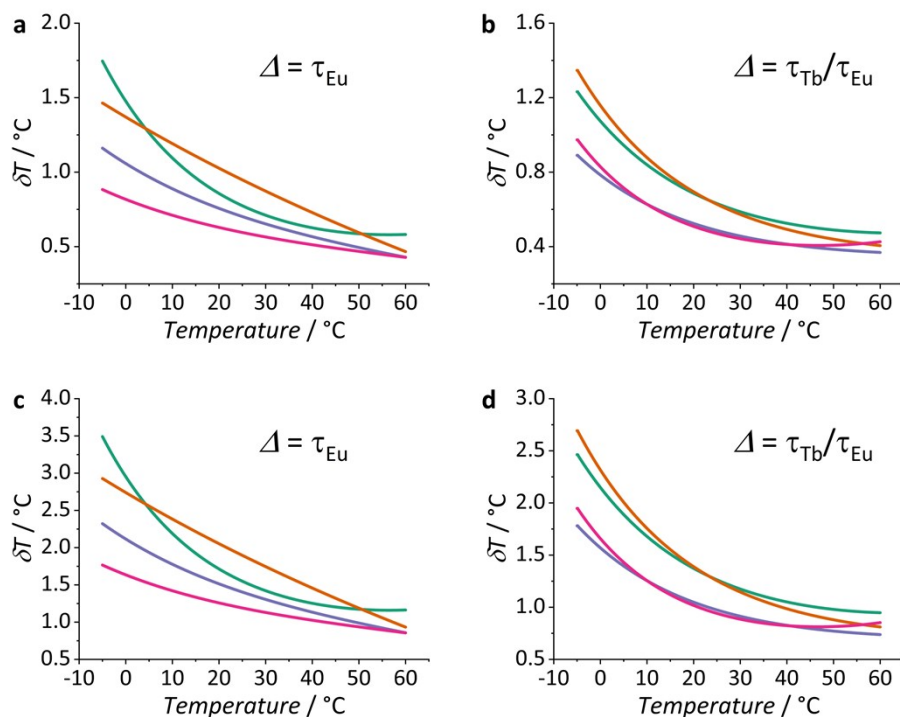


Figure S11. Temperature uncertainty (δT) curves of $\{\text{Eu}_1\text{Tb}_{19}\}$ (green), $\{\text{Eu}_2\text{Tb}_{18}\}$ (orange), $\{\text{Eu}_3\text{Tb}_{17}\}$ (purple) and $\{\text{Eu}_4\text{Tb}_{16}\}$ (pink) MCAs, for both single (τ_{Eu}) and ratiometric ($\tau_{\text{Tb}}/\tau_{\text{Eu}}$) approaches, considering **a-b** 1% and **c-d** 2% of instrumental error.

Table S3. Best-fitting parameters for thermometric parameters.

MCA / Δ	A_1	A_2	x_0	p	r^2
$\{\text{Eu}_1\text{Tb}_{19}\} / \tau_{\text{Tb}}/\tau_{\text{Eu}}$ ratio	0.78	17.06	398.56	11.19	0.999
$\{\text{Eu}_2\text{Tb}_{18}\} / \tau_{\text{Tb}}/\tau_{\text{Eu}}$ ratio	0.41	1110.31	611.99	11.48	0.999
$\{\text{Eu}_3\text{Tb}_{17}\} / \tau_{\text{Tb}}/\tau_{\text{Eu}}$ ratio	0.20	644.14	601.14	11.21	0.999
$\{\text{Eu}_4\text{Tb}_{16}\} / \tau_{\text{Tb}}/\tau_{\text{Eu}}$ ratio	0.11	1.71	359.75	13.46	0.999
$\{\text{Eu}_1\text{Tb}_{19}\} / \tau_{\text{Eu}}$	1.49	0.20	308.96	12.39	0.999
$\{\text{Eu}_2\text{Tb}_{18}\} / \tau_{\text{Eu}}$	1.90	-157.88	1895.08	2.73	0.998
$\{\text{Eu}_3\text{Tb}_{17}\} / \tau_{\text{Eu}}$	1.52	-0.26	310.82	7.51	0.999
$\{\text{Eu}_4\text{Tb}_{16}\} / \tau_{\text{Eu}}$	1.51	-0.11	289.94	7.68	0.999

Table S4. Thermometric performance of selected thermometers, employing lifetime (τ) as thermometric parameter (Δ).

System	Δ	$\Delta T / ^\circ\text{C}$	$S_{R\text{max}} / \% ^\circ\text{C}^{-1}$	$T_{\text{max}} / ^\circ\text{C}$	Reference
{Ln ₂₀ }	τ_{Eu}	-5 to 60	2.3	60	This work
{Ln ₂₀ }	$\tau_{\text{Tb}}/\tau_{\text{Eu}}$	-5 to 60	2.7	60	This work
Gd ₂ O ₂ S:Eu	τ_{Eu}	0 to 60	4.5	0	2
Eu _{0.6} Tb _{1.4} Pt ₃ complex	$\tau_{\text{Tb}}/\tau_{\text{Eu}}$	-123 to 27	3.3	-34	3
Ba ₂ LaTaO ₆ :Eu	τ_{Eu}	20 to 440	0.2	240	4
[Eu(bzac) ₃ (H ₂ O) ₂]	τ_{Eu}	-190 to 20	1.4	20	5
[Eu(CPDK ₃₋₅) ₃ phen]	τ_{Eu}	25 to 75	1.6	75	6
[Eu(tta) ₃ (pyphen)]	τ_{Eu}	-190 to 50	1.7	50	7

References

- [1] C. D. S. Brites, S. Balabhadra and L. D. Carlos, *Adv. Opt. Mater.*, 2019, **7**, 1801239.
- [2] N. Katumo, G. Gao, F. Laufer, B. S. Richards and I. A. Howard, *Adv. Opt. Mater.*, 2020, **8**, 2000507.
- [3] M. Wyczesany, J. J. Zakrzewski, B. Sieklucka and S. Chorazy, *J. Mater. Chem. C*, 2022, **10**, 12054–12069.
- [4] Y. Hua, T. Wang, J. S. Yu and P. Du, *Mater. Today Chem.*, 2022, **25**, 100945.
- [5] D. A. Gállico, I. O. Mazali and F. A. Sigoli, *J. Lumin.*, 2017, **192**, 224–230.
- [6] D. V. Lapaev, V. G. Nikiforov, V. S. Lobkov, A. A. Knyazev and Y. G. Galyametdinov, *Opt. Mater.*, 2018, **75**, 787–795.
- [7] F. M. Cabral, D. A. Gállico, I. O. Mazali and F. A. Sigoli, *Inorg. Chem. Commun.*, 2018, **98**, 29–33.